THE UNIVERSITY of EDINBURGH

Edinburgh Research Explorer

Melt inclusion constraints on the magma source of Eyjafjallajökull 2010 flank eruption

Citation for published version:
Moune, S, Sigmarsson, O, Schiano, P, Thordarson, T & Keiding, JK 2012, 'Melt inclusion constraints on the magma source of Eyjafjallajökull 2010 flank eruption', *Journal of Geophysical Research*, vol. 117, no. 2. https://doi.org/10.1029/2011JB008718

Digital Object Identifier (DOI):
10.1029/2011JB008718

Link:
Link to publication record in Edinburgh Research Explorer

Document Version:
Publisher's PDF, also known as Version of record

Published In:
Journal of Geophysical Research

Publisher Rights Statement:
Published in Journal of Geophysical Research: Solid Earth by the American Geophysical Union (2012)

General rights
Copyright for the publications made accessible via the Edinburgh Research Explorer is retained by the author(s) and / or other copyright owners and it is a condition of accessing these publications that users recognise and abide by the legal requirements associated with these rights.

Take down policy
The University of Edinburgh has made every reasonable effort to ensure that Edinburgh Research Explorer content complies with UK legislation. If you believe that the public display of this file breaches copyright please contact openaccess@ed.ac.uk providing details, and we will remove access to the work immediately and investigate your claim.

OPEN ACCESS

Download date: 05. May. 2023

Melt inclusion constraints on the magma source of Eyjafjallajökull 2010 flank eruption

S. Moune,[1] O. Sigmarsson,[1,2] P. Schiano,[1] T. Thordarson,[3] and J. K. Keiding[4]

Received 26 July 2011; revised 23 December 2011; accepted 27 December 2011; published 24 February 2012.

[1] The 2010 eruptive activity at the Eyjafjallajökull volcanic system began 20 March with a basaltic flank eruption on a 300 m long fissure on the Fimmvörðuháls Pass, in between Eyjafjallajökull and Mýrdalsjökull volcanoes. The magma expelled from the fissure is olivine- and plagioclase-bearing mildly alkali basalt that exhibits uniform and rather primitive whole-rock composition. This event provides a rare opportunity to assess deep magmatic processes in Iceland. Melt inclusions (MIs) hosted in olivine phenocrysts were analyzed for their major, trace and volatile element concentrations to enable identification of magmatic source(s) for Eyjafjallajökull volcano and to better constrain processes occurring at depth. The MIs, in particular those in Mg-rich olivines, record primary magma composition before homogenisation and differentiation during magma ascent. The olivine phenocrysts hosting the MIs have a large compositional range, extending from Fo_{73} to Fo_{87}, reflecting changes in the magma characteristics from the source to the surface. The MI compositions exhibit significant variations with MgO ranging from 5.2 to 7.2 wt%. This compositional range was caused by a binary mixing of two basaltic end-members followed by fractional crystallization process. The sources of these end-members are identical to those of Katla and Surtsey basalts, with a dominant role of the Katla source. Trace element characteristics of the Fimmvörðuháls MIs suggest important proportions of recycled oceanic crust in their mantle sources.

Citation: Moune, S., O. Sigmarsson, P. Schiano, T. Thordarson, and J. K. Keiding (2012), Melt inclusion constraints on the magma source of Eyjafjallajökull 2010 flank eruption, *J. Geophys. Res.*, *117*, B00C07, doi:10.1029/2011JB008718.

1. Introduction

[2] Eyjafjallajökull volcano is located at the southern tip of the Eastern Volcanic Zone (Figure 1), which currently is the most active part of the Neovolcanic zones in Iceland [*Thordarson and Larsen*, 2007]. The 2010 activity at Eyjafjallajökull volcano began 20 March by a basaltic flank event along a 300 m long fissure trending N36°E on the western flanks of the Fimmvörðuháls Pass, which forms the saddle between Eyjafjallajökull and Mýrdalsjökull volcanoes (Figure 1). It featured up to 15 lava fountains, which reached heights of 50–150 m and produced tephra fall that formed a continuous 70-m-high cone constructed around the active vents and a thin tephra blanket extending up to 1–2 km from the source. Late on 31 March a new fissure opened at an angle of ∼50° to the original fissure (trending ∼N15°W). Shortly thereafter, on 2 April, it became the loci of the eruptive activity. The activity produced a small a'a lava flow field accompanied by efficient degassing. The lava that was discharged to the north in open channels formed spectacular lava falls when it cascaded into deep gullies carved in the basement of Eyjafjallajökull volcano. The flank eruption ended on 12 April having produced approximately 0.025 km^3. The erupted magma was mildly alkali olivine- and plagioclase-phyric basalt with fairly uniform whole-rock composition with MgO of ∼8.5 ± 0.3 wt%, a composition similar to that produced in the 1963–67 Surtsey eruption [*Sigmarsson et al.*, 2011].

[3] Basaltic eruptions in Iceland are most frequently associated with high-level magma chambers (i.e., depth of 2–6 km) at central volcanoes producing basalts of evolved compositions. Eruptions of primitive basalts (MgO > 7%) are infrequent with the last one occurring during 1963–67 at Surtsey in the Vestmannaeyjar archipelago only 60 km south of Eyjafjallajökull [e.g., *Jakobsson*, 1979; *Furman et al.*, 1991; *Sigmarsson*, 1996] (Figure 1). The geobarometry on the Fimmvörðuháls flank eruption shows that this initial phase of the Eyjafjallajökull eruption was tapped from a deep-seated magma reservoir of a depth of approximately 16–18 km [*Keiding and Sigmarsson*, 2012]. The flank eruption of relatively primitive basalt at Fimmvörðuháls thus presents an occasion to study deeper magmatic processes than is possible through more evolved basalts in Iceland. In order to discuss the magma generation of Fimmvörðuháls basalts, melt inclusions (MIs) were analyzed for major, trace and

[1]Laboratoire Magmas et Volcans, Université Blaise Pascal, CNRS-IRD, Clermont-Ferrand, France.
[2]Institute of Earth Science, Nordvolc, University of Iceland, Reykjavik, Iceland.
[3]Grant Institute, School of GeoScience, University of Edinburgh, Edinburgh, UK.
[4]German Research Centre for Geosciences, Potsdam, Germany.

Copyright 2012 by the American Geophysical Union.
0148-0227/12/2011JB008718

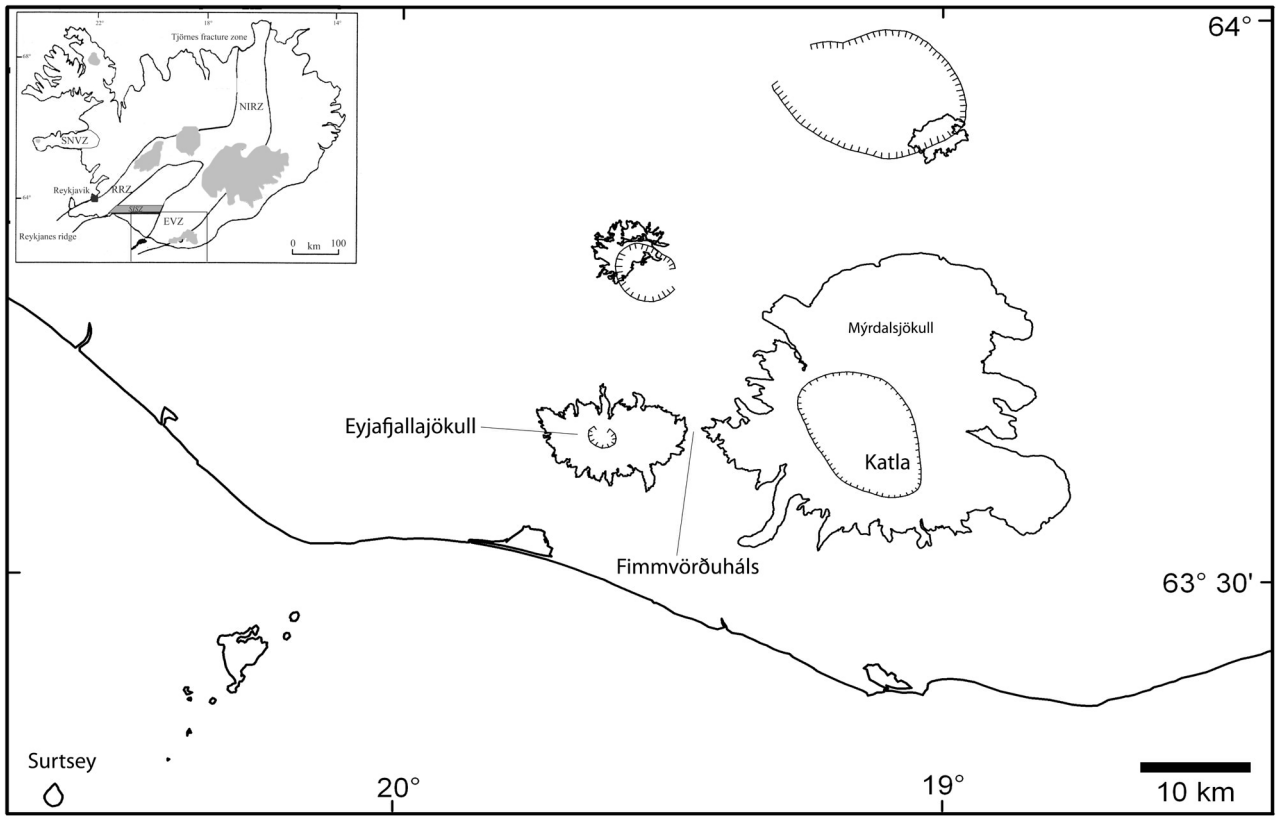

Figure 1. Simplified map of the basaltic flank eruption site at Fimmvörðuháls Pass, between the ice caps Eyjafjallajökull and Mýrdalsjökull. The subglacial volcano Katla and the island of Surtsey are also shown. Inset: the Neovolcanic zones of Iceland (EVZ: Eastern Volcanic Zone, RRZ: Reykjanes Rift Zone, SNVZ Snæfellsnes Volcanic Zone, NIRZ: North Icelandic Rift Zone and SISZ: South Iceland Seismic Zone).

volatile element concentrations. Melt inclusions in minerals, especially Mg-rich olivines, have been shown to record primary magma composition before homogenization and differentiation during magma ascent [e.g., *Schiano*, 2003].

2. Sample Description and Preparation

[4] Lapilli-sized tephra (sample FH-2) that fell on fresh snow during the night of 24 March, was collected the day after approximately 100 m south of the main crater on the Fimmvörðuháls eruption fissure. The basalt contains euhedral phenocrysts of olivine, plagioclase and clinopyroxene, which occur frequently as glomerocrysts. The compositions of the phenocrysts range from $Fo_{71–87}$, $An_{73–86}$ and Mg#70–76, respectively, whereas more evolved compositions and oscillatory zonations are observed in those forming glomerocrysts ($Fo_{57–68}$, $An_{76–68}$, Mg#79–65). The glass composition shows slight but significant variations (MgO: 4.09–4.67%; TiO_2: 4.82–5.31%; K_2O: 1.00–1.17%; average on 21 analyses is given in Table 1). Olivine crystals were hand-picked under binoculars from the 600–1000 μm grain size fraction of crushed tephra. Melt inclusion bearing crystals were selected and washed with acetone, embedded in epoxy and polished individually to produce adequate exposure of the MIs for in situ microanalysis. The MIs are randomly scattered throughout the host olivine crystals and typically spherical to oblate in shape with a diameter in the range of 15–60 μm (Figure 2). Most inclusions contain shrinkage bubbles caused by the greater thermal contraction of the melt compared to the host mineral during post-entrapment cooling (Figure 2 and Table 1). Because they were naturally quenched during the eruption, most of the MIs are totally deprived of daughter minerals (see *Anderson* [1974] and *Lowenstern* [2003] for definition). Post-entrapment reactions that occurred inside the inclusions are restricted to limited crystallization of the host phase on inclusion walls (Table 1). Note that some melt inclusions from the FH-2 sample contain both glass and minute sulfides. However, no sulfide globule was observed under the microscope in any of the analyzed glass inclusions (Figure 2).

3. Analytical Methods

3.1. Electron Microprobe

[5] Major and volatile (S, Cl, F) element compositions of host minerals and MIs were measured on a SX-100 CAMECA electron microprobe (EMP) at Laboratoire Magmas et Volcans (LMV, Clermont-Ferrand) using 15 kV accelerating voltage. Sample currents and counting times used for analyzing different groups of elements are listed in Table 2a. A mixture of mineral standards (synthetic and natural) and glasses (A-THO and VG2) was used for calibration (see *Oladottir et al.* [2011] for further details).

Table 1. Melt Inclusion (MI) in Olivine, Whole-Rock and Groundmass Major and Volatile Compositions (in wt%) in Fimmvörðuháls Basalt (FH-2)[a]

Samples	SiO_2	TiO_2	Al_2O_3	FeO*[b]	MnO	MgO	CaO	Na_2O	P_2O_5	K_2O	Cl	S	F	H_2O	Sum	Fo[c]	PEC[d] (%)	Bubble
Whole-rock	46.2	3.04	15.1	15.2	0.18	8.19	10.0	2.73	0.41	0.56	–	–	–	0.08[e]	99.00			
Groundmass	46.5	5.00	13.1	14.6	0.23	4.52	9.62	3.31	0.71	1.06	–	–	–	–	98.6			
A1	46.7	3.56	13.9	13.6	0.18	5.23	8.25	3.81	0.55	1.02	0.241	0.189	0.078	–	97.4	72.8	1.3	Yes
A2	44.8	3.93	14.0	14.5	0.19	5.77	9.25	3.65	0.63	0.96	0.075	0.170	0.065	–	97.9	73.5	2.3	Yes
A4	50.8	2.96	15.1	6.59	0.09	6.32	12.7	2.86	0.29	0.52	0.025	0.090	0.051	0.95	99.3	87.0	1.8	Yes
A5	49.7	3.01	15.2	6.95	0.13	6.54	12.8	2.77	0.30	0.51	0.028	0.098	0.051	–	98.1	86.8	3	Yes
A6-1	46.4	3.31	15.6	10.7	0.17	6.19	10.4	3.35	0.47	0.72	0.049	0.115	0.069	–	97.5	80.1	2.7	Yes
A7-1	45.1	4.07	13.9	13.9	0.14	5.97	9.80	2.96	0.47	0.82	0.058	0.154	0.064	–	97.4	74.9	3	No
A7-2	46.8	3.41	14.3	12.4	0.23	5.29	9.60	3.49	0.58	0.97	0.062	0.140	0.055	–	97.3	74.9	2	Yes
A8	47.0	3.34	14.8	10.7	0.12	6.52	11.3	2.77	0.32	0.48	0.028	0.125	0.056	–	97.5	80.9	2.8	No
B1-1	46.8	3.43	14.5	11.6	0.18	6.17	10.6	3.14	0.38	0.49	0.041	0.140	0.071	0.89	98.5	78.7	2.6	Yes
B2	46.3	3.45	14.7	11.7	0.11	6.20	10.6	3.00	0.59	0.77	0.074	0.167	0.064	0.82	98.5	78.7	2	Yes
B6	48.4	2.88	15.7	10.6	0.19	5.45	9.95	3.68	0.39	0.50	0.022	0.109	0.086	–	97.9	78.2	1.2	No
C3	46.5	3.50	15.8	11.2	0.18	5.40	9.45	3.85	0.72	0.88	0.072	0.151	0.070	–	97.9	77.1	1.3	Yes
C4	44.1	5.24	14.8	12.0	0.19	6.13	11.2	2.85	0.34	0.63	0.092	0.128	0.049	–	97.8	78.0	2.4	No
C5	48.5	2.95	15.9	9.53	0.08	5.52	10.7	3.54	0.25	0.36	0.024	0.106	0.058	–	97.5	80.2	1.1	No
C7	47.4	3.31	15.7	8.06	0.04	7.21	12.4	2.87	0.43	0.67	0.035	0.123	0.049	–	98.3	86.1	4.1	No
D1-1	48.9	2.97	15.6	6.66	0.11	5.94	12.7	2.68	0.26	0.49	0.025	0.094	0.035	–	96.5	86.1	0.9	Yes
D1-2	47.0	3.16	16.2	6.85	0.13	6.13	12.8	2.95	0.37	0.59	–	–	–	–	96.2	86.1	1.4	Yes
D2	49.2	3.08	15.6	6.88	0.14	6.16	12.3	2.86	0.34	0.43	0.021	0.081	0.048	–	97.2	86.8	2	Yes
D3	48.2	2.94	16.2	8.96	0.10	5.67	11.3	2.93	0.40	0.48	0.021	0.106	0.048	–	97.4	81.6	0.7	Yes
D4	49.6	3.13	15.2	9.24	0.26	5.33	10.9	2.93	0.34	0.45	0.020	0.105	0.045	–	97.6	80.1	1.1	Yes
E1	49.0	3.11	16.2	6.38	0.12	6.01	12.8	2.91	0.34	0.56	0.027	0.118	0.049	0.99	98.6	86.9	0.6	Yes
E2	48.9	3.09	15.8	10.4	0.25	6.00	10.2	3.41	0.35	0.50	0.022	0.101	0.077	–	99.1	80.1	1.9	Yes
E3	46.5	3.63	14.5	11.7	0.21	6.33	9.76	3.47	0.40	0.90	0.062	0.121	0.059	–	97.6	78.9	5.7	No
E4	46.3	3.35	16.2	10.0	0.22	6.08	9.51	3.05	0.36	0.58	0.027	0.107	0.060	–	95.9	80.8	3.3	No
E5	45.5	3.88	15.7	9.78	0.11	6.89	10.9	3.01	0.38	0.56	0.025	0.105	0.051	–	97.0	83.0	3.9	No
E6	51.0	3.20	15.3	6.53	0.19	6.23	12.3	2.61	0.37	0.41	0.022	0.077	0.047	–	98.2	86.9	1.3	Yes

[a]Dash means not determined.
[b]Total iron as FeO.
[c]Fo (mol%) represent the host mineral compositions.
[d]PEC is the percentage of post-entrapment host olivine crystallization on MI rims.
[e]Loss in ignition (LOI) in wt%.

[6] A focused beam of 1 μm diameter was used for mineral analysis but in order to reduce Na loss, a 5–10 μm defocused beam was employed during glass analysis. Analyses of Cl, S and F were preformed with 80 nA sample current and 50 s acquisition time using the LPET diffraction crystal (Cl and S) and 300 s on three TAP crystals (F, Table 2a). In order to minimize volatile losses during analysis, the beam was blanked regularly with the Faraday cup and counts were collected in 20 s intervals by 5 iterations. Variations in the wavelength of sulfur Kα X-ray as a function of its oxidation state in silicate glasses were taken into account during the sulfur analysis [*Carroll and Rutherford*, 1988; *Métrich and Clocchiatti*, 1996]. The EMP precision (2σ) is better than 5% for major elements, except MnO, Na_2O, K_2O and P_2O_5 where it is less than 10%. The estimated 2σ precision for Cl, S and F is 7%, 4% and 28%, respectively. Both reproducibility and accuracy were established by replicate analyses of VG-A99 glass standard [*Jarosewich et al.*, 1979; *Thornber et al.*, 2002] (Table 2b) for major-element concentrations, Alvin glass standard [*Métrich and Clocchiatti*, 1989, 1996; *Mosbah et al.*, 1991; *Straub and Layne*, 2003] for S concentrations, and Ke12 glass standard [*Métrich and*

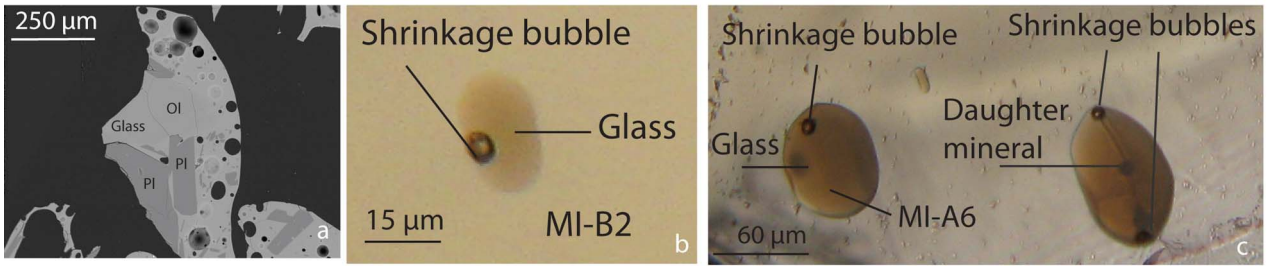

Figure 2. (a) Backscattered-electron images of individual tephra grain from Fimmvörðuháls eruption showing glass and homogeneous crystals (Ol: olivine, Pl: plagioclase). (b) Melt inclusion in olivine Fo < 80 showing only glass and a shrinkage bubble. (c) Melt inclusions in olivine Fo ≥ 80: The inclusion to the left contains only glass and a shrinkage bubble, whereas that to the right MI contains two shrinkage bubbles and visible daughter minerals. Only MIs without daughter minerals were analyzed in this study.

Table 2a. Analytical Conditions for EMP Measurements[a]

	Sample Current (nA)	Diffraction Crystal Types				
		LLIF	LPET	TAP	TAP	TAP
Minerals	15	Fe (30)	K (10) Ti (10) Ca (10)	Si (10) Mg (20) Si (10)	Na (10) Al (10)	
Melt inclusions	8	Fe (40) Mn (30)	K (40) Ti (10) Ca (10) P (10)	Mg (20)	Na (10) Al (20)	
	80		S (50) Cl (50)	F (100)	F (100)	F (100)

[a]Counting times in seconds are given in parentheses.

Rutherford, 1991] for Cl and F concentrations. Measured values of 0.100 ± 0.003 wt% for S in Alvin, 0.34 ± 0.01 wt% for Cl and 0.47 ± 0.03 wt% for F in Ke12 are in good agreement with the published accepted values of these standards. Two points were measured in most melt inclusions and the average is given in Table 1, except for the smallest melt inclusions where only one point could be measured. Each olivine grain was analyzed twice, one point was measured near the MI and one far from the MI to check compositional homogeneity. For most olivines, both analyses are within the standard deviation (2σ). If the olivine is zoned (such as E3), the closest measurement to the analyzed MI was considered to assess equilibrium between MI and host crystal.

3.2. Laser-Ablation Inductively Coupled-Plasma Mass-Spectrometry (LA-ICP-MS)

[7] Trace element analyses of MIs were performed at the Laboratoire Magmas et Volcans (Clermont-Ferrand) with a Resonetics M50 EXCIMER laser (193 nm wavelength) coupled to an Agilent 7500cs ICP-MS. The laser was operated at 6 mJ energy, 2 Hz repetition rate and an 11 μm spot size diameter. Analytical details as well as reproducibility and accuracy are given by *Sigmarsson et al.* [2011]. Trace element compositions are given in Table 3.

3.3. Ion Probe

[8] Ion Probe analyses of water concentrations were performed on a Cameca 4f SIMS instrument at the University of Edinburgh in a few melt inclusions following the procedures detailed by *Humphreys et al.* [2008]. Calibration was

Table 2b. Standard Reproducibility and Estimated Accuracy of Major Elemental Analysis[a]

Samples	VG-A99 Mean (±SD)	VG-A99[b]
SiO2	51.02 (0.24)	50.9
TiO2	4.15 (0.06)	4.06
Al2O3	12.52 (0.09)	12.5
FeO	13.26 (0.25)	13.3
MnO	0.14 (0.10)	0.15
MgO	5.06 (0.04)	5.08
CaO	9.09 (0.08)	9.30
Na2O	2.76 (0.12)	2.66
K2O	0.85 (0.03)	0.820
P2O5	0.43 (0.07)	0.380
Sum	99.29 (0.49)	99.2

[a]Standard deviation is given in parentheses.
[b]Recommended values for VG-A99 reference material [*Jarosewich et al.*, 1979; *Thornber et al.*, 2002].

Table 3. Melt Inclusion (MI) Trace Element Compositions (in ppm) in Olivine From Fimmvörðuháls Basalt (FH-2)[a]

Samples	Rb	Ba	Th	U	Nb	Ta	La	Ce	Sr	Pr	Nd	Sm	Zr	Hf	Eu	Gd	Tb	Dy	Y	Ho	Er	Yb	Lu
A1	24.8	237	2.57	1.12	33.0	2.11	25.7	61.7	435	7.92	37.8	8.56	237	5.98	2.69	8.00	1.09	6.39	33.3	1.28	3.59	2.89	0.311
A1	23.8	230	2.65	0.990	31.6	1.86	25.3	59.1	421	7.45	34.8	7.73	236	5.32	2.15	7.73	0.957	6.28	32.4	1.38	3.54	2.94	0.487
A6-1	13.0	168	1.47	0.583	27.2	1.60	19.6	49.7	472	6.42	30.7	6.71	189	4.35	2.27	6.03	0.949	5.91	26.2	1.02	2.75	2.51	0.260
A8	8.89	98.6	1.00	0.516	18.4	1.23	14.8	38.3	429	5.58	27.1	6.35	167	4.05	2.37	6.98	1.01	6.19	26.7	1.08	2.84	2.35	0.364
C5	4.66	74.6	0.55	0.300	15.4	0.87	11.8	31.9	423	4.67	26.5	6.27	150	4.40	2.18	5.59	0.880	5.54	26.2	0.96	2.59	3.56	0.268
C7	14.5	153	1.64	0.681	23.2	1.42	19.2	46.6	465	6.30	27.9	6.39	163	4.13	2.30	5.87	0.933	5.75	25.7	1.08	2.65	2.22	0.311
D1-1	9.71	99.1	1.04	0.590	16.4	1.02	15.4	35.8	368	5.04	24.5	6.18	158	3.94	2.27	5.23	1.01	5.21	25.1	1.05	2.60	1.89	0.244
D1-1	10.3	103	1.12	0.310	16.2	1.16	15.5	37.7	370	5.19	22.9	6.66	152	4.47	1.98	5.85	1.00	4.68	25.7	1.06	2.38	1.94	0.238
D1-2	12.0	128	1.32	0.360	19.3	1.21	17.6	40.4	427	5.49	25.8	5.79	164	4.27	2.28	7.02	0.944	5.46	24.4	1.07	2.71	1.83	0.352
D3	8.59	95.6	1.27	0.451	14.9	1.05	15.4	38.2	408	5.47	27.4	6.40	175	7.86	2.29	6.57	1.10	5.97	27.7	0.979	2.66	2.43	0.350
D4	8.22	93.2	1.24	0.498	16.0	1.08	16.4	40.9	407	5.71	29.3	7.27	189	5.23	2.57	7.11	1.06	5.45	25.0	1.01	2.43	2.05	0.197
E2	7.83	94.7	1.25	<ld	18.1	1.22	16.1	40.8	415	5.29	28.2	6.88	192	4.28	2.43	7.97	0.87	6.46	30.5	1.21	2.89	2.15	<ld
E3	19.0	184	1.66	0.465	23.9	1.62	22.7	52.2	427	6.82	31.9	7.88	204	5.33	2.70	7.81	1.09	6.53	30.5	1.30	2.99	2.46	0.315
E4	10.4	118	1.45	0.547	17.3	1.14	17.0	41.1	473	5.39	26.4	6.20	177	4.76	2.21	6.13	0.915	5.38	24.8	1.04	2.43	2.30	0.269
E5	7.86	98.2	1.41	0.551	18.7	1.34	17.5	41.6	390	5.82	27.3	6.46	179	4.74	2.60	7.40	1.08	5.34	26.2	1.13	2.52	2.43	0.252
E6	7.57	85.2	1.14	0.381	16.4	1.04	15.6	36.4	362	4.85	23.6	6.06	169	4.60	2.21	6.57	1.05	6.32	27.7	1.11	2.52	2.25	0.364

[a]Here <ld means below detection limit.

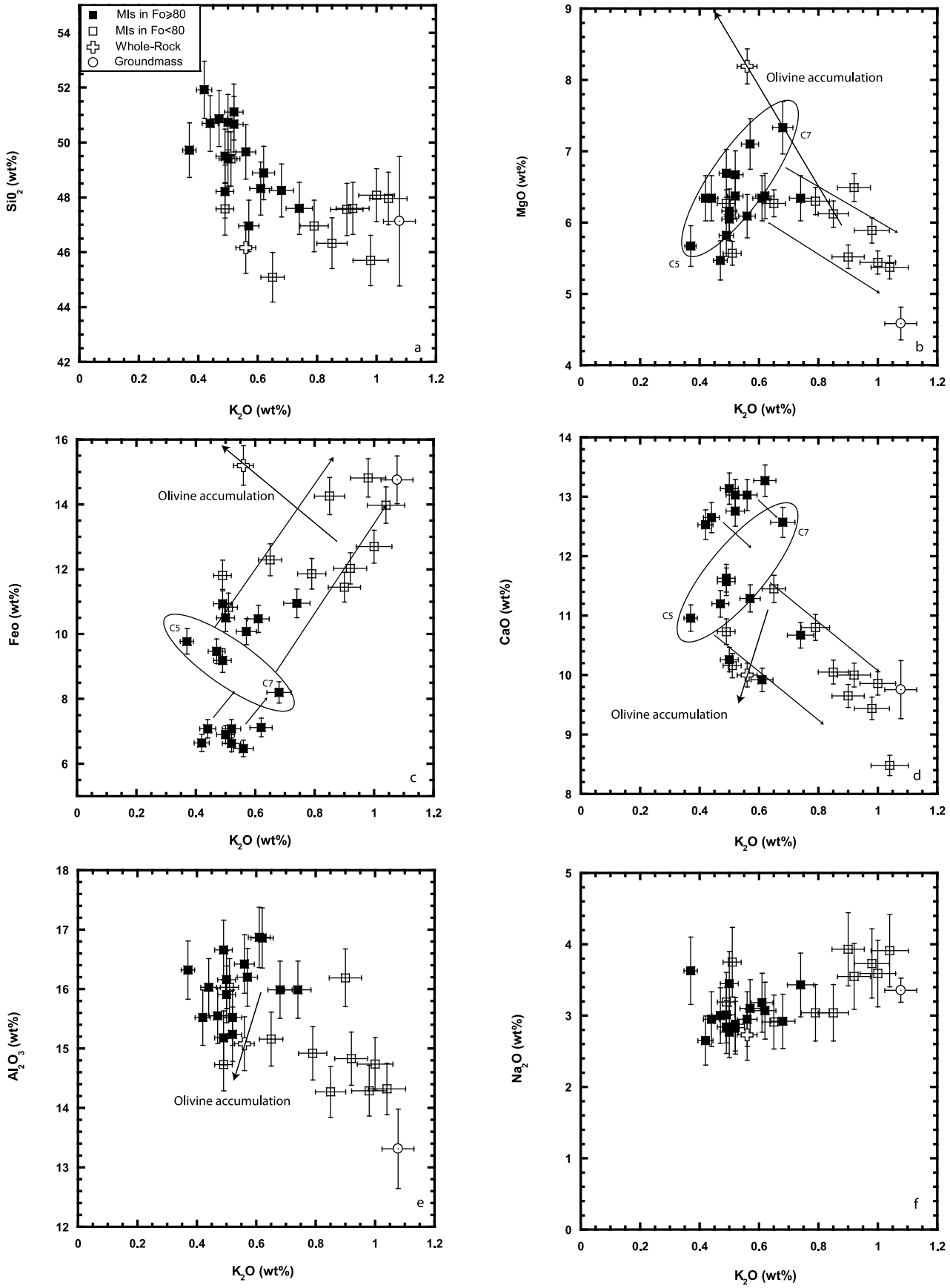
MIs in Fo≥80
MIs in Fo<80
Whole-Rock
Groundmass
Si0$_2$ (wt%)
MgO (wt%)
Feo (wt%)
CaO (wt%)
Al$_2$O$_3$ (wt%)
Na$_2$O (wt%)
K$_2$O (wt%)
Olivine accumulation
C5
C7
a
b
c
d
e
f

Figure 3

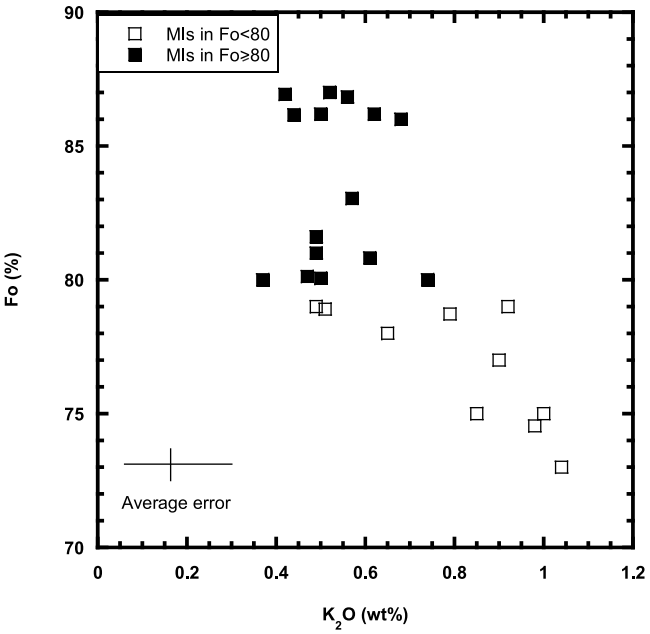

Figure 4. Correlation between K_2O concentration (wt%) of melt inclusions in the FH-2 basalt and the corresponding host olivine composition (Fo%). Average 2σ error is plotted.

performed using rhyolitic and basaltic glasses with known water concentrations. The water concentrations of the reference glasses bracket the sample concentrations. The estimated 2σ precision for H_2O is 10%.

3.4. Post-entrapment Modifications and Correction for Late-Stage Crystallization

[9] In principle, the compositions of MIs could be modified by the diffusion of Fe from the melt into the host mineral and diffusion of Mg from the crystal into the liquid during re-equilibration of the overgrowth rim with the host mineral [e.g., *Danyushevsky et al.*, 2000, 2002; *Gaetani and Watson*, 2002]. However, such potential Fe-Mg diffusion would result in significantly higher melt-olivine equilibrium constant K_D $(=(FeO/MgO)_{ol}/(FeO/MgO)_{melt})$ between ferrous iron and magnesium [*Roeder and Emslie*, 1970; *Toplis*, 2005] than the well established value of 0.3. The Fimmvörðuháls results, in contrast, have apparent K_D very close to 0.3 or somewhat lower. Moreover, the FeO content of the MIs of Fimmvörðuháls basalts does not vary with size. Finally, MIs with low Fe contents were trapped in olivine with high Fo composition (Fo86–87, Figure 3) suggesting negligible post-entrapment Fe diffusion. Therefore, we conclude that diffusion-controlled mechanisms did not play a significant role in modifying the major element composition of the MIs of Fimmvörðuháls basalts.

[10] In order to obtain the original liquid composition, the MI analysis must be corrected for potential host crystallization on the MI rims after melt entrapment. For olivine-hosted inclusions, this correction is based on the iron and magnesium equilibrium between olivine and basaltic melt. However, the relative proportions of Fe_2O_3 and FeO in the melts are unknown. A Fe_2O_3/FeO value of 0.14 measured in Surtsey basalts [*Sigmarsson et al.*, 2009], which has major-element composition indistinguishable from those of Fimmvörðuháls basalts [*Sigmarsson et al.*, 2011], is adopted here. A fixed value of 0.3 for the Fe-Mg K_D was used to compute, by dissolving numerically 0.1 wt% increments of olivine into the melt, the equilibrium composition between different host olivines and corresponding MI. This permitted to estimate the amount of post-entrapment crystallization (PEC in % in Table 1), which ranges from 0.6 to 5.7%. The MI analyses were corrected for this crystallization and the resulting compositions are given in Table 1.

4. Results

[11] The FH-2 tephra emitted from the flank eruption at Fimmvörðuháls has a MgO content of 8.2 wt% (Table 1). This relatively primitive basalt with a mildly alkali character presents a rare opportunity to assess deep magma characteristics. The whole rock and the glass composition are generally within the range of the MIs (Table 1 and Figure 3), with the exception of higher MgO and FeO concentrations in whole-rock indicating an accumulation of ~10% of olivines (Figure 3). Such accumulation of olivines is also consistent with the Na_2O, Al_2O_3, K_2O and SiO_2 concentrations of the whole-rock. Based on the melt-olivine Fe-Mg equilibrium constant, K_D of 0.3 the bulk magma composition is in equilibrium with olivine Fo_{75}. All olivine crystals hosting melt inclusions analyzed in this study are euhedral and of homogeneous composition, with the exception of olivine E3 that presents a zonation from Fo_{79} to Fo_{86}. The compositional range of the host olivines is rather large from Fo_{87} to Fo_{73} reflecting magma evolution from the source to the surface.

[12] After correction for post-entrapment crystallization, the compositions of the MIs show significant variations with, for instance, MgO concentrations ranging from 5.23 to 7.21 wt% (Table 1). Compositions of MIs in the same olivine show a small variability (for instance K_2O range 0.82–0.97 wt% in A7–1/A7–2 and 0.49–0.59 wt% in D1–1/D1–2), whereas the overall compositional range of the MIs is large (K_2O ranging from 0.36 to 1.02 wt%) in comparison with that of the host olivine compositions (Figure 4). No clear differentiation trend emerges from the major element variations in the MIs (Figure 3). However, based on trace element systematics, two distinct MI populations can be identified (see below). Hence, the whole data set is divided into two groups depending on the forsterite content of their host olivines (MIs in Fo ≥ 80 and MIs in Fo < 80) and major

Figure 3. Major element concentrations of (a) SiO_2, (b) MgO, (c) FeO, (d) CaO, (e) Al_2O_3, and (f) Na_2O versus that of K_2O in wt% showing the compositional variations of melt inclusions (MIs) in the Fimmvörðuháls FH-2 basalt. The whole rock and the groundmass compositions are also shown. In Figures 3b, 3c and 3d, ellipses are drawn around melt inclusions, which composition represent magma mixing between two end-members (C5 and C7). Black lines represent various differentiation trends between the most primitive (Fo ≥ 86) and primitive MIs (80 < Fo < 86), and between the latter ones and the evolved MIs (Fo < 80). Trend of olivine accumulation explaining the Fe and Mg concentrations of the whole-rock is also shown (see text for details). Results are normalized to 100%. Error bars are given at 95% confidence level.

element concentrations will be presented and discussed separately for the two groups. The compositions of MIs trapped in olivines Fo < 80 show decreasing olivine Fo content, stable SiO_2, decreasing Al_2O_3, CaO and MgO and increasing FeO and Na_2O concentrations with increasing K_2O concentration (Figures 3 and 4). The MIs compositional spread shows that a single liquid line of decent cannot explain the melt evolution that may suggest several parental magmas for the evolved compositions. The major element composition of the most evolved olivine-hosted MIs (in terms of K_2O content: A1 and A2 with K_2O = 1.02 and 0.96 wt%, respectively; Table 1) is indistinguishable to those of plagioclase-hosted MIs [*Thordarson et al.*, 2011], which record more advanced differentiation stage of the Fimmvörðuháls basalt. In contrast, the more primitive MIs, trapped in olivines with Fo ≥ 80, show a more complex evolution where SiO_2 concentration decreases, Al_2O_3 and Na_2O remain stable and MgO increases with increasing K_2O concentrations. Both CaO and FeO vary considerably without any clear relationships to the K_2O concentrations.

[13] Concentrations of Cl, S, F and H_2O in MIs are in the range of 204–2470 ppm, 783–1939 ppm, 359–878 ppm and 0.82–0.99 wt%, respectively. The most primitive melt inclusions (i.e., trapped in olivines 80 ≤ Fo < 87) contain an average of 1058 ppm S, 273 ppm Cl, 542 ppm F and 0.97 wt% H_2O. On diagrams showing volatile element concentrations as a function of those of K_2O, the more evolved MIs plot on differentiation vectors from the MIs in olivines with Fo ≥ 80 that extrapolate through the origin (Figure 5). Melt inclusions in plagioclases ($An_{69–70}$) from the same sample [*Thordarson et al.*, 2011] yield even more evolved compositions and plot on same differentiation vectors. The volatile elements thus confirm the observation that major element concentrations may reflect more than one differentiation trend. It is worth noting that very few MIs seem to have trapped a melt already degassed in sulfur or water (Figures 5a and 5d). Finally, Cl concentration of A2, and to a lesser extent C4 and B2, plot far above the differentiation vectors (Figure 5c and Table 1) indicating either that this inclusion is recording chlorine-brine-rich melt or a xenocrystic olivine with consistent S and F volatile concentrations but exceptionally high Cl. A significant assimilation of Cl-rich material through crustal contamination is not supported by the $\Delta^{18}O$ values of Fimmvörðuháls samples, which range between 5.4‰ and 5.8‰ and correspond to mantle values [*Sigmarsson et al.*, 2011]. At present this high Cl value remains enigmatic. The volatile concentrations of the MIs in more primitive olivines (Fo ≥ 80) show less variability whereas their ratios to that of K_2O is close to what is observed in the more evolved MIs.

[14] Trace element composition of the MIs varies considerably. The most incompatible elements show similar evolution as K_2O with a variation in composition over a factor of three (e.g., Rb concentration ranges from 7.57 ppm to 24.8 ppm, Figure 6 and Table 3). This is in stark contrast to relatively uniform whole-rock composition of the Fimmvörðuháls basalts (e.g., Rb-range: 11.9–12.8 ppm [*Sigmarsson et al.*, 2011]), which is well within the compositional range of the MIs. This enhanced concentration variability, offered by the MI results, gives access to finer details of the deep-seated magmatic processes. In general, the Fimmvörðuháls MIs have trace element characteristics in between those of basalts from the neighboring volcanoes in the Eastern Volcanic Zone, namely Surtsey and Katla (Figures 1 and 7).

[15] A notable feature of the MIs trace element patterns is positive spikes in HFS-elements such as Nb and Ta (Figure 7), which are opposite to those of continental crust and arc-type lavas [*Hofmann*, 1988]. Moreover, although characterized by an overall enrichment in incompatible trace elements, the mantle-normalized patterns of the MIs display significant depletions in the LIL-elements such as U, Th, Ba and Rb.

5. Discussion

5.1. Do the MIs Represent Undegassed Magma at Depth?

[16] Melt inclusions trapped in early formed minerals, such as magnesian olivine phenocrysts, are potentially undegassed and therefore could hold clues to the primitive volatile composition of the erupted magma [e.g., *Métrich and Wallace*, 2008]. However, MIs may form in minerals crystallizing from partially degassed magma, MIs may leak if fractures are present [*Lowenstern*, 1995], hydrogen may diffuse out of the inclusion and fast-diffusion species may enter from the melt around the host crystals into the MIs [e.g., *Massare et al.*, 2002; *Cottrell et al.*, 2002; *Portnyagin et al.*, 2008; *Chen et al.*, 2011]. In this study, only MIs with no visible fracture or dislocation boundaries were chosen for analyses.

[17] Hydrogen diffusion out of the olivine during natural cooling of the sample cannot be excluded and such diffusion might explain the low water content of B2 (see Figure 5d). Alternatively, this MI represents a partially H_2O degassed melt. The facts that the average Cl/K_2O of all inclusions is close to the value of 0.06 ± 0.02, typical for Icelandic basalts (Cl/K_2O = 0.04) [*Jambon et al.*, 1995], the H_2O, F and Cl concentrations and S/Cl are close to those from other mantle-plume related magmas (e.g., S/K_2O = 0.05–0.4, S/Cl = 0.5–6 [*Schilling et al.*, 1980; *Dixon and Clague*, 2001; *Lassiter et al.*, 2002; *Métrich et al.*, 2004]) implies negligible degassing of the MIs. In addition, their water concentration and H_2O/K_2O (except for B2) are also consistent with those measured in subglacial basaltic glasses from Iceland, which are likely to reflect the juvenile water concentrations (H_2O/K_2O = 0.1–2 [*Nichols et al.*, 2002]). These arguments allow us to assume that most of the MIs represent undegassed melts with juvenile S, Cl, F and H_2O concentrations.

5.2. Magmatic Processes at Depth

[18] Variations in major element concentrations clearly result from more than a single magmatic process at depth. To discriminate between various processes such as partial melting, fractional crystallization and magma mixing, the trace element concentrations and ratios can be very useful [e.g., *Schiano et al.*, 2010, and references therein]. The mantle source appears homogeneous since both Sr and Nd isotope ratios are constant in the Fimmvörðuháls basalts [*Sigmarsson et al.*, 2011]. However, such constancy of isotope ratios measured in whole-rocks could as well be due to thorough mixing and homogenisation of melts from different sources with variable isotope ratios [*Sigmarsson et al.*, 2000]. Co-variations of trace element ratios and concentrations such

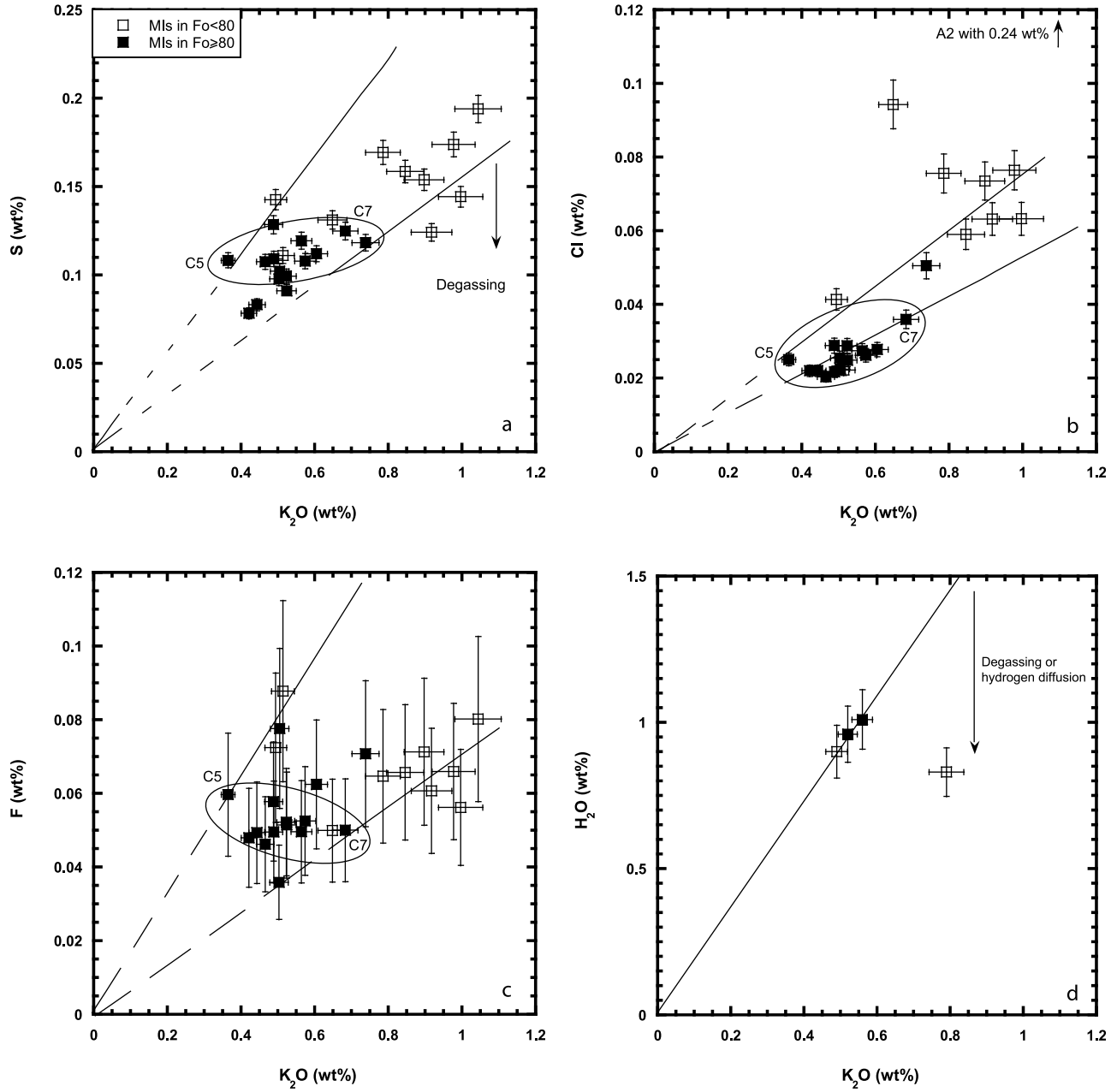

Figure 5. (a–d) Evolution of the dissolved volatile concentrations in Fimmvörðuháls melt inclusions (MIs) as a function of K_2O concentration. Ellipses represent the mixing process between two end-members (C5 and C7). Black lines denote differentiation vectors from the mixed basaltic melt with more than one differentiation trends, extrapolated through the origin, necessary to explain the whole data set. A few of the more evolved MIs seem to have trapped a melt already degassed in water and sulfur (Figures 5a and 5d). Melt inclusions with lowest S concentrations might represent melts that have experienced early sulphur immiscibility. The highest Cl values measured in melt inclusion A2 fall above the differentiation vector indicating either an inclusion recording chlorine-brine-rich melt or a xenocrystic olivine (Figure 5b). The scattering of the F results is due to the large error associated with F measurements (∼28%, Figure 5c). All results are normalized to 100%. Error bars show 2σ errors.

as Ba/Sm versus Ba, Rb/Nd versus Rb, La versus Th and Ba versus K_2O reveal two very distinct processes (Figure 6).

[19] The whole data set define linear correlations between concentrations of highly incompatible trace elements that do not extrapolate through the origin, contrary to what is expected during fractional crystallization (Figures 6a and 6b). Furthermore, when reported in C_A/C_B versus C_A diagram (where C_A and C_B are the concentrations of A, a highly incompatible element, and B, a moderately incompatible element) the MIs in olivines rich in Fo (Fo ≥ 80) define trends that are consistent with series of magma batches produced by different degrees of partial melting or mixing of different

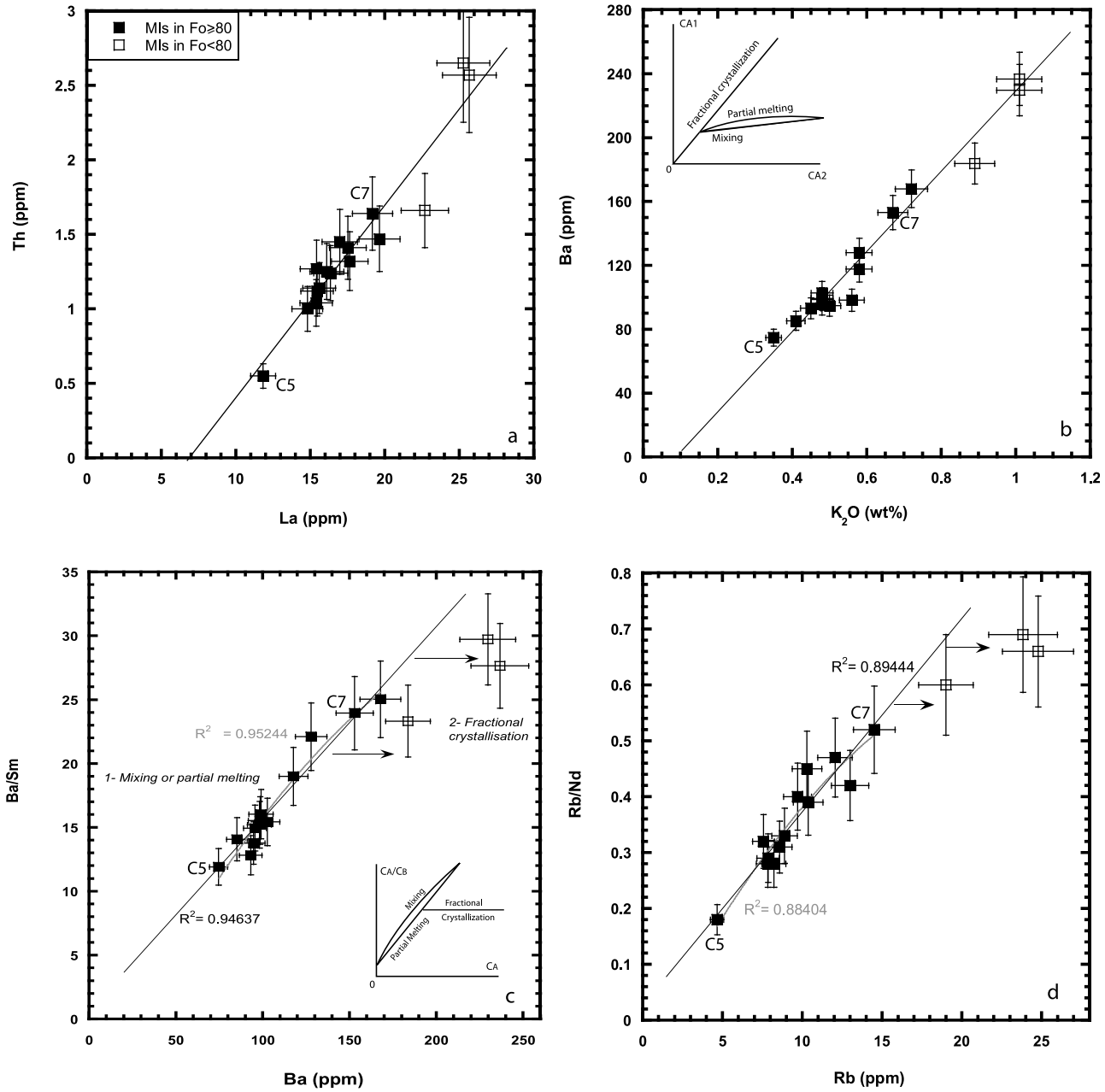

Figure 6. (a, b) Highly incompatible trace element variation diagrams for melt inclusions (MIs) in olivines from Fimmvörðuháls basalts. The results define linear correlations that do not pass through the origin. Figure 6b shows a schematic CA_1 versus CA_2 diagram (with CA_1 and CA_2 being two highly incompatible elements) with curve showing calculated melt composition produced by fractional crystallization, partial melting and mixing processes. (c, d) Plots of Ba/Sm versus Ba and Rb/Nd versus Rb for MIs from Fimmvörðuháls. The MIs in Fo-rich olivines (Fo > 80) define arrays that are both consistent with a series of magma batches produced by different degrees of partial melting (gray curve and R^2) and mixing (black line and R^2; see text for further discussion). The MIs in olivines with Fo < 80 produce almost horizontal trends reflecting a simple fractional crystallization process. Figure 6c shows a schematic CA/CB versus CA diagram (with CA and CB are the concentrations of A, a highly incompatible element, and B, a moderately incompatible element) showing theoretical correlation curves during fractional crystallization, partial melting and mixing processes. C5 and C7 that represent the two end-members of the mixing process are also shown.

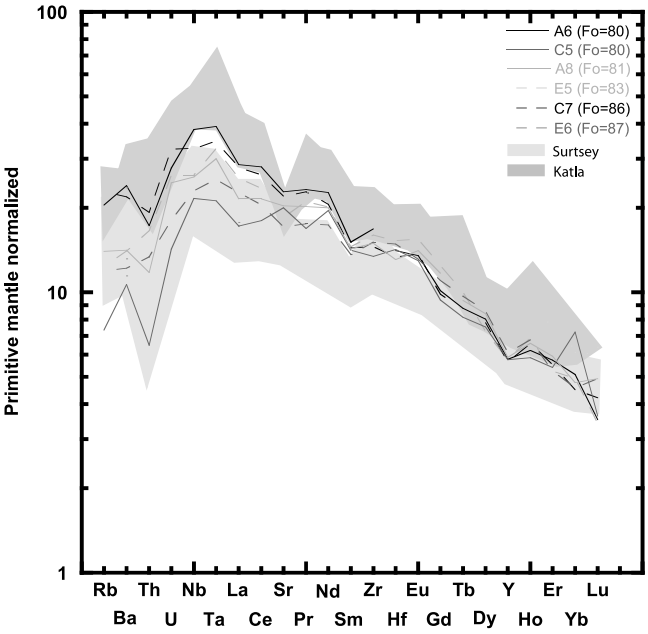

Figure 7. Primitive mantle normalized diagram showing trace element data for a few primitive melt inclusions (Fo > 80) from Fimmvörðuháls basalts along with whole-rock analysis on Katla and Surtsey basalts in dark and light gray fields, respectively [*Furman et al.*, 1991; *Lacasse et al.*, 2007].

melts (Figures 6c and 6d). It should be noted that, in such diagrams, horizontal lines define fractional crystallization, linear trends with a positive slope define partial melting process of a single magma source whereas hyperbolic curves are consistent with a binary magma mixing. Regression coefficients (R^2) close to unity for both straight lines and hyperbolic curves (Figures 6c and 6d) do not permit to distinguish between mixing and partial melting processes from diagrams in Figure 6. However, even if an increase in the degree of melting by a factor of 2 could in principle account for the twofold variations of highly incompatible element concentrations such as K_2O (0.36–0.72 wt%) or Ba (75–168 ppm) (assuming a bulk partition coefficient close to 0 for these elements), such a limited variation in the degree of melting cannot explain the concomitant wide spread in the Fo contents of the host olivine phenocrysts ($80 \leq Fo < 87$). Indeed, experimental results demonstrate that an increase in the degree of melting of peridotite and pyroxenite by a factor of 4.5–5 and 2.5–4, respectively, is needed to account for such a large variation in the Fo content of the olivine in equilibrium with the melt [*Lambart et al.*, 2009; *Baker and Stolper*, 1994]. Consequently, the compositional variability of our primitive MIs is best explained by mixing between two end-members of basaltic compositions.

[20] The more evolved MIs (in Fo < 80) define almost horizontal trends in Figures 6c and 6d as expected for melt compositions generated by fractional crystallization. Using mass balance algorithms from *Störmer and Nicholls* [1978], we determined that these trends result from ~35% of fractionation of 11% olivines $Fo_{80–75}$, 62% plagioclases $An_{70–80}$ and 27% augites from the more primitive mixed basaltic melt (with a sum of squared residuals equal to 0.04).

[21] Taken together, trace element constraints suggest that mixing of diverse basaltic melts is recorded in the more primitive MIs, with concomitant fractional crystallization producing the melt of the more evolved MIs.

5.3. Source of Fimmvörðuháls Basalts

[22] In order to better constrain the source of the mixing end-members at the origin of the Fimmvörðuháls parental basalts, we focus our discussion only on the more primitive MIs (MIs in $Fo \geq 80$).

[23] Primitive-mantle normalized trace element spectra are shown in Figure 7 and are, not surprisingly, typical of hot spot basalts. For clarity purposes, only six MIs are plotted. However, all the spectra display very similar trends, the main difference being variable concentration of the trace elements and the fact that the most incompatible elements are the most variable. Melt inclusions with the most and the least enriched trace element spectra (C7 and C5, respectively) represent the two end-members of the deep mixing process at the origin of Fimmvörðuháls basalts. Trace element spectra from two neighboring volcanoes (Surtsey and Katla) are plotted in Figure 7. It is clear that the spectra of Fimmvörðuháls basalts are enclosed between those of these two volcanoes: Katla basalts comparing favorably with the most enriched end-member (C7) and Surtsey basalts with the least enriched end-member (C5) of the mixing process beneath Fimmvörðuháls.

[24] These two end-members (represented by C5 and C7) can also be identified from variation of volatile elements in Figure 5. Mixing between these two end-members followed by fractional crystallization trends explains the MIs with variable volatile-potassium ratios. Furthermore, the identification of the two end-members, of the binary magma mixing at depth, is also clear from major-element compositions as can be seen from diagrams of FeO, CaO and MgO versus K_2O (Figures 4b–4d). In these diagrams, the compositional spread of MIs in $Fo \geq 80$, generated by variable mixing proportions, is at the origin of different fractional crystallization trends as recorded in the more evolved inclusions. However, it is notable that the most primitive MIs (in $Fo_{86–87}$) show a restricted but distinct range in FeO and CaO concentrations that appears to be linked to the C7 end-member composition. Indeed, these most primitive compositions could be the parental magma to the Katla-like mixing end-member. The presence of these primitive MI suggests a dominant role of the Katla-like source for the Fimmvörðuháls basalts. This is not surprising given the proximity to the Katla volcanic system (Figure 1). The same relationship between Katla- and Surtsey-type basalts producing the parental magma for the Fimmvörðuháls basalts is also observed in Figure 8, where the data show a very good linear correlation ($R^2 = 0.99$) between highly incompatible trace element concentrations (e.g., La versus Ce, Figure 8a), which does not extrapolate through the origin. The dominant role of the Katla basalts in the source of the nearby Eyjafjallajökull basalts (as represented by those of Fimmvörðuháls) is also supported by the quantification of the mixing proportions relative to Katla magma source in Figure 8a. Indeed, considering the most primitive whole-rock composition from Surstey and Katla, the two end-members of the basaltic mixing C5 and C7 are quantified to represent ~30% and ~90% of Katla parental magmas, respectively. Primitive MIs of Fimmvörðuháls

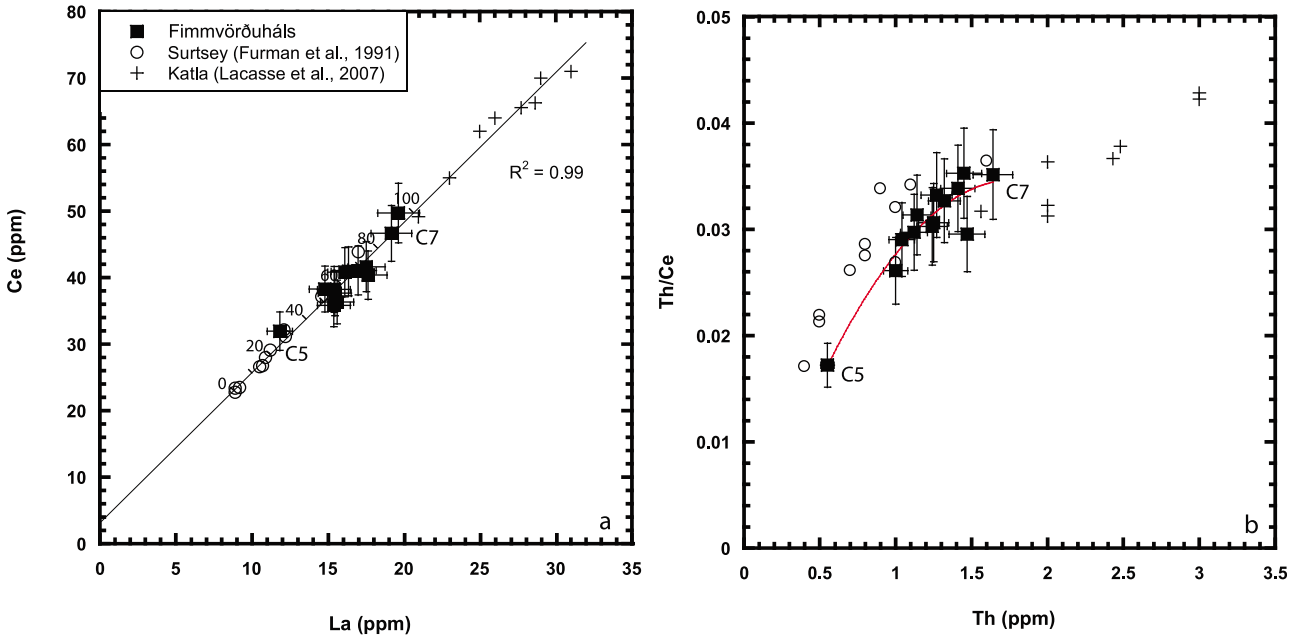

Figure 8. Comparison between Katla, Surtsey and Fimmvörðuháls basalts [*Furman et al.*, 1991; *Lacasse et al.*, 2007]. (a) Highly incompatible trace element variation diagram (La versus Ce) in melt inclusions (MIs) from Fimmvörðuháls along with whole-rock data from Katla and Surtsey. The data define correlations that do not pass through the origin. Mixing percentage of the Katla end-member is calculated from the most primitive whole-rock analyses of Surstey and Katla basalts. (b) Plots of Th/Ce versus Ce for MIs from Fimmvörðuháls along with whole-rock data from Katla and Surtsey. A binary mixing curve between the two end-members (C5 and C7) is shown.

represent thus a compositional range of ~50 to 90% of Katla parental magmas.

[25] The mixing of melts derived from mantle sources similar to those under Surtsey and Katla volcanoes is confirmed by curved relationships in Figure 8b. In Figure 8b, C5 and C7 have respectively the same Th/Ce as observed in basalts from Surtsey and Katla. The difference in trace element ratios between these three volcanoes is consistent with isotope ratios indicating mantle source heterogeneity beneath this part of the Neovolcanic zones in Iceland [*Sigmarsson et al.*, 1992, 2000; *Kokfelt et al.*, 2006]. Moreover, whole-rock isotope ratios of Fimmvörðuháls basalts, which could be interpreted to reflect a homogeneous mantle source, can also be explained by a thorough mixing and homogenisation of different mantle melts. Indeed, the isotope ratios of Sr and Nd of Fimmvörðuháls basalts fall in between those of Katla and Surstey basalts [*Sigmarsson et al.*, 2008, 2011]. Therefore, the trace element compositions of the MIs reveal deep magma processes undetectable by whole-rock geochemical criteria.

[26] The trace element patterns of the melt inclusions (Figure 7) are characterized by a general inverted V-shape with a continuous decrease in the normalized abundances of the most highly incompatible elements, U to Rb. Such a depletion of the most incompatible elements is characteristic of all ocean-island basalts with a HIMU-type isotope signature (i.e., radiogenic Pb isotope ratios) and thought to reflect a link between the origin of HIMU-type ocean-island basalts and mid-ocean ridge basalt (MORB) mantle sources [see *Hofmann*, 1997, and references therein]; that is, the depletions on the left side of these patterns are consistent with a derivation from a source that is likely to incorporate large proportions of subduction-zone processed, recycled oceanic crust. This is also consistent with the proposition of recycled crust in the form of garnet pyroxenite in the mantle source of the southern end of the Eastern Volcanic Zone, where basalts are characterized by elevated Pb-isotope ratios [e.g., *Kokfelt et al.*, 2006; *Sigmarsson et al.*, 2008].

5.4. Primitive Volatile Source of Eyjafjallajökull: Comparison With Other EVZ Basalts

[27] The primitive flank magmas of Eyjafjallajökull volcano, erupted at the Fimmvörðuháls Pass and recorded in MIs in olivines with Fo > 80, have an average volatile content of 1058 ppm S, 273 ppm Cl, 542 ppm F and 0.98 wt% H_2O. These volatile contents can be shown to be coherent with the tectonic setting of the volcano. In the S/Cl versus 1/Cl diagram (Figure 9), MIs from basalts of the Eastern Volcanic Zone show a regular geographical variation with the highest values at the center of Iceland and lower values toward the south along the volcanic zone. Indeed, samples from the Vestmannaeyjar islands (Surtsey and Heimaey) have the lowest S/Cl, those from Hekla and Katla plot close to the proposed hot spot values of *Métrich et al.* [1991], whereas MIs from Laki and Veidivötn tholeiites form a linear array between this presumed hot spot and higher MORB values [*Métrich et al.*, 1991; *Thordarson et al.*, 1996, 2003; *Moune et al.*, 2007]. This range is easily explained by the fact that variable mixtures of mantle melts from the Iceland plume and the depleted upper mantle reservoir (such as MORB) are at

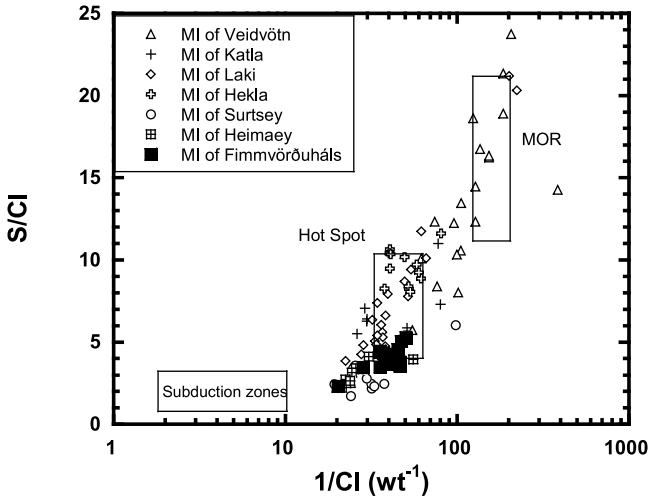

Figure 9. The S/Cl values versus 1/Cl for melt inclusions (MIs) of Fimmvörðuháls basalts compared to those from the EVZ of Iceland [*Métrich et al.*, 1991; *Thordarson et al.*, 1996, 2003; *Moune et al.*, 2007]. The thin boxes outline the proposed compositional fields for MIs from volcanoes of hot spots, mid-ocean ridges (MOR) and subduction zones as defined by *Métrich et al.* [1991]. The MIs from Fimmvörðuháls plot between those of Surtsey and Katla (see text for further discussion).

the origin of Icelandic basalts [*Schilling*, 1973; *Sigmarsson and Steinthórsson*, 2007, and references therein].

[28] The Fimmvörðuháls results plot at values in between those of Surtsey and Katla confirming the major- and trace element constraints for magma mixing at their origin.

6. Conclusion

[29] The flank eruption of relatively primitive basalt at Fimmvörðuháls presents a rare opportunity to assess deep magmatic processes in Iceland. The major, trace and volatile element compositions of MIs in the basalt can be explained by a mixing process between two basaltic end-members followed by fractional crystallization. The two end-members are related to the parental magmas of Katla and that of Surtsey, with a dominant presence of the Katla one in the magma source of Fimmvörðuháls. Trace element features suggest that the mantle source of Fimmvörðuháls contains older segments of recycled oceanic crust.

[30] **Acknowledgments.** We thank N. Métrich and M. Portnyagin for constructive reviews that led to significant improvements in the manuscript. We are grateful to Jean-Luc Devidal for assistance with EPM and LA-ICP-MS measurements, Mhammed Benbakkar for the whole-rock analysis, Armann Höskuldsson and Thorsteinn Jónsson for help during sample collection. N. Cluzel and F. Sorbardère are acknowledged for their help in preparing the MIs. A French INSU-CNRS program CT-2 grant and a grant from the Icelandic Research Fund (110242011 "Volcano Anatomy") covered the analytical cost. J.K. thanks the Carlsberg Foundation. This is Laboratory of Excellence ClerVolc contribution 7.

References

Anderson, A. T. (1974), Chlorine, sulfur, and water in magmas and oceans, *Geol. Soc. Am. Bull.*, *85*, 1485–1492, doi:10.1130/0016-7606(1974)85<1485:CSAWIM>2.0.CO;2.

Baker, M. B., and E. M. Stolper (1994), Determining the composition of high-pressure mantle melts using diamond aggregates, *Geochim. Cosmochim. Acta*, *58*, 2811–2827, doi:10.1016/0016-7037(94)90116-3.

Carroll, M. R., and M. J. Rutherford (1988), Sulfur speciation in hydrous experimental glasses of varying oxidation state: Results from measured wavelength shifts of sulfur X-rays, *Am. Mineral.*, *73*, 845–849.

Chen, Y., A. Provost, P. Schiano, and N. Cluzel (2011), The rate of water loss from olivine-hosted melt inclusions, *Contrib. Mineral. Petrol.*, *162*, 625–636, doi:10.1007/s00410-011-0616-5.

Cottrell, E., M. Spiegelmann, and C. H. Langmiur (2002), Consequences of diffusive reequilibration for the interpretation of melt inclusions, *Geochem. Geophys. Geosyst.*, *3*(4), 1026, doi:10.1029/2001GC000205.

Danyushevsky, L. V., F. N. Della-Pasqua, and S. Sokolov (2000), Re-equilibration of melt inclusions trapped by magnesian olivine phenocrysts from subduction-related magmas: petrological implications, *Contrib. Mineral. Petrol.*, *138*, 68–83, doi:10.1007/PL00007664.

Danyushevsky, L. V., A. W. McNeill, and A. V. Sobolev (2002), Experimental and petrological studies of melt inclusions in phenocryst from mantle-derived magmas: an overview of techniques, advantages and complications, *Chem. Geol.*, *183*, 5–24, doi:10.1016/S0009-2541(01)00369-2.

Dixon, J. E., and D. A. Clague (2001), Volatiles in basaltic glasses from Loihi Seamount, Hawaii; evidence for a relatively dry plume component, *J. Petrol.*, *42*, 627–654, doi:10.1093/petrology/42.3.627.

Furman, T., F. A. Frey, and K. H. Park (1991), Chemical constraints on the petrogenesis of mildly alkaline lavas from Vesmannaeyjar, Iceland: The Eldfell (1973) and Surtsey (1963–1967) eruptions, *Contrib. Mineral. Petrol.*, *109*, 19–37, doi:10.1007/BF00687198.

Gaetani, G. A., and E. B. Watson (2002), Modeling the major-element evolution of olivine-hosted melt inclusions, *Chem. Geol.*, *183*, 25–41, doi:10.1016/S0009-2541(01)00370-9.

Hofmann, A. W. (1988), Chemical differentiation of the Earth: The relationship between mantle, continental crust, and oceanic crust, *Earth Planet. Sci. Lett.*, *90*, 297–314, doi:10.1016/0012-821X(88)90132-X.

Hofmann, A. W. (1997), Mantle geochemistry: The message from oceanic volcanism, *Nature*, *385*, 219–229, doi:10.1038/385219a0.

Humphreys, M. C. S., T. Menand, J. D. Blundy, and K. Klimm (2008), Magma ascent rates in explosive eruptions: Constraints from H_2O diffusion in melt inclusions, *Earth Planet. Sci. Lett.*, *270*, 25–40.

Jakobsson, S. P. (1979), Petrology of recent basalts from the eastern volcanic zone, Iceland, *Acta Nat. Isl.*, *26*, 1–103.

Jambon, A., B. Déruelle, G. Dreibus, and F. Pineau (1995), Chlorine and bromine abundance in MORB: The contrasting behaviour of the Mid-Atlantic Ridge and East Pacific Rise and implications for chlorine geodynamic cycle, *Chem. Geol.*, *126*, 101–117, doi:10.1016/0009-2541(95)00112-4.

Jarosewich, E., J. A. Nelen, and J. A. Norberg (1979), *Electron Microprobe Reference Samples for Mineral Analysis*, *Smithson. Inst. Contrib. Earth Sci.*, vol. 22, edited by R. F. Fudali, pp. 68–78, Smithson. Inst. Press, Washington, D. C.

Keiding, J., and O. Sigmarsson (2012), Geothermobarometry of the 2010 Eyjafjalljökull eruption: New constraints on Icelandic magma plumbing systems, *J. Geophys. Res.*, doi:10.1029/2011JB008829, in press.

Kokfelt, T. F., K. Hoernle, F. Hauff, J. Fiebig, R. Werner, and D. Garbe-Schoenberg (2006), Combined trace element and Pb-Sr-Nd-O isotope evidence for recycled oceanic (upper and lower) crust in the Icelandic plume, *J. Petrol.*, *47*, 1705–1749, doi:10.1093/petrology/egl025.

Lacasse, C., H. Sigurdsson, S. N. Carey, H. Johannesson, L. E. Thomas, and N. W. Rogers (2007), Bimodal volcanism at the Katla subglacial caldera, Iceland: Insight into the geochemistry and petrogenesis of rholitic magmas, *Bull. Volcanol.*, *69*, 373–399.

Lambart, S., D. Laporte, and P. Schiano (2009), An experimental study of pyroxenite partial melts at 1 and 1.5 GPa: Implications for the major element composition of mid-ocean ridge basalts, *Earth Planet. Sci. Lett.*, *288*, 335–347, doi:10.1016/j.epsl.2009.09.038.

Lassiter, J. C., E. Hauri, I. K. Nikogosian, and H. G. Barsczus (2002), Chlorine-potassium variations in melt inclusions from Raivavae and Rapa, Austral Islands: Constraints on chlorine recycling in the mantle and evidence for brine-induced melting of oceanic crust, *Earth Planet. Sci. Lett.*, *202*, 525–540, doi:10.1016/S0012-821X(02)00826-9.

Lowenstern, J. B. (1995), Applications of silicate-melt inclusions to the study of magmatic volatiles, in *Magmas, Fluid and Ore Deposits*, edited by J. H. F. E. Thompson, *Short Course Ser. Mineral. Soc. Can.*, *23*, 71–99.

Lowenstern, J. B. (2003), Melt inclusions come of age: Volatiles, volcanoes, and Sorby's legacy, in *Melt Inclusions in Volcanic Systems: Methods, Applications and Problems*, edited by B. De Vivo and R. J. Bodnar, pp. 1–21, Elsevier, Amsterdam, doi:10.1016/S1871-644X(03)80021-9.

Massare, D., N. Métrich, and R. Clocchiatti (2002), High-temperature experiments on silicate melt inclusions in olivine at 1 atm: Inference on

temperatures of homogenization and H_2O concentrations, *Chem. Geol.*, *183*, 87–98, doi:10.1016/S0009-2541(01)00373-4.

Métrich, N., and R. Clocchiatti (1989), Melt inclusion investigation of the volatile behaviour in historic alkali basaltic magmas of Etna, *Bull. Volcanol.*, *51*, 185–198, doi:10.1007/BF01067955.

Métrich, N., and R. Clocchiatti (1996), Sulfur abundance and its speciation in oxidized alkaline melts, *Geochim. Cosmochim. Acta*, *60*, 4151–4160, doi:10.1016/S0016-7037(96)00229-3.

Métrich, N., and M. J. Rutherford (1991), Experimental study of chlorine behaviour in hydrous silicic melts, *Geochim. Cosmochim. Acta*, *56*, 606–616.

Métrich, N., and P. J. Wallace (2008), Volatile abundances in basaltic magmas and their degassing paths tracked by melt inclusions, *Rev. Mineral. Geochem.*, *69*, 363–402, doi:10.2138/rmg.2008.69.10.

Métrich, N., H. Sigurdsson, P. S. Meyer, and J. D. Devine (1991), The 1783 Lakagigar eruption in Iceland: Geochemistry, CO_2 and sulfur degassing, *Contrib. Mineral. Petrol.*, *107*, 435–447, doi:10.1007/BF00310678.

Métrich, N., P. Allard, N. Spilliaert, D. Andronico, and M. Burton (2004), 2001 flank eruption of the alkali- and volatile-rich primitive basalt responsible for Mount Etna's evolution in the last three decades, *Earth Planet. Sci. Lett.*, *228*, 1–17, doi:10.1016/j.epsl.2004.09.036.

Mosbah, M., R. Clocchiatti, J. Tiria, J. Gosset, P. Massiot, and P. Trocellier (1991), Study of hydrogen in melt inclusions trapped in quartz with a nuclear microprobe, *Nucl. Instrum. Methods*, *54*, 298–303, doi:10.1016/0168-583X(91)95529-M.

Moune, S., O. Sigmarsson, T. Thordarson, and P. J. Gauthier (2007), Recent volatile evolution in the magmatic system of Hekla volcano, Iceland, *Earth Planet. Sci. Lett.*, *255*, 373–389, doi:10.1016/j.epsl.2006.12.024.

Nichols, A. R. L., M. R. Carroll, and A. Hoskuldsson (2002), Is the Iceland hot spot also wet? Evidence from the water contents of undegassed submarine and subglacial pillow basalts, *Earth Planet. Sci. Lett.*, *202*, 77–87, doi:10.1016/S0012-821X(02)00758-6.

Oladottir, B., O. Sigmarsson, G. Larsen, and J.-L. Devidal (2011), Provenance of basaltic tephra from Vatnajökull subglacial volcanoes, Iceland, as determined by major- and trace-element analyses, *Holocene*, *21*, 1037–1048, doi:10.1177/0959683611400456.

Portnyagin, M., R. Almeev, S. Matveev, and F. Holtz (2008), Experimental evidence for rapid water exchange between melt inclusions in olivine and host magma, *Earth Planet. Sci. Lett.*, *272*(3–4), 541–552, doi:10.1016/j.epsl.2008.05.020.

Roeder, E., and R. F. Emslie (1970), Olivine-liquid equilibrium, *Contrib. Mineral. Petrol.*, *29*, 275–289, doi:10.1007/BF00371276.

Schiano, P. (2003), Primitive mantle magmas recorded as silicate melt inclusions in igneous minerals, *Earth Sci. Rev.*, *63*, 121–144, doi:10.1016/S0012-8252(03)00034-5.

Schiano, P., M. Monzier, J. P. Eissen, H. Martin, and K. T. Koga (2010), Simple mixing as the major control of the evolution of volcanic suites in the Ecuadorian Andes, *Contrib. Mineral. Petrol.*, *160*, 297–312, doi:10.1007/s00410-009-0478-2.

Schilling, B. G. (1973), Iceland mantle plume: Geochemical study of Reykjanes ridge, *Nature*, *242*, 565–571, doi:10.1038/242565a0.

Schilling, B. G., M. B. Bergeron, and R. Evans (1980), Halogens in the mantle beneath the North Atlantic, *Philos. Trans. R. Soc. London, Ser. A*, *297*, 147–178, doi:10.1098/rsta.1980.0208.

Sigmarsson, O. (1996), Short magma chamber residence time at an Icelandic volcano inferred from U-series disequilibria, *Nature*, *382*, 440–442, doi:10.1038/382440a0.

Sigmarsson, O., and S. Steinthórsson (2007), Origin of Icelandic basalts: A review of their petrology and geochemistry, *J. Geodyn.*, *43*, 87–100, doi:10.1016/j.jog.2006.09.016.

Sigmarsson, O., M. Condomines, and S. Fourcade (1992), A detailed Th, Sr and O isotope study of Hekla: Differentiation processes in an Icelandic volcano, *Contrib. Mineral. Petrol.*, *112*, 20–34, doi:10.1007/BF00310953.

Sigmarsson, O., H. Karlsson, and G. Larsen (2000), The 1996 and 1998 subglacial eruptions beneath Vatnajökull glacier in Iceland: Contrasting geochemical and geophysical inferences on magma migration, *Bull. Volcanol.*, *61*, 468–476.

Sigmarsson, O., J. Maclennan, and M. Carpentier (2008), Geochemistry of igneous rocks in Iceland: A review, *Joekull*, *58*, 139–160.

Sigmarsson, O., T. Thordarson, and S. P. Jakobsson (2009), Segregations in Surtsey lavas (Iceland) reveal extreme magma differentiation during late stage flow emplacement, in *Studies in Volcanology: The Legacy of George Walker*, *Spec. Publ. Int. Assoc. Volcanol. Chem. Earth's Inter.*, vol. 2, edited by T. Thordarson et al., pp. 85–104, Geol. Soc., London.

Sigmarsson, O., I. Vlastelic, R. Andreasen, I. Bindeman, J.-L. Devidal, S. Moune, J. K. Keiding, G. Larsen, A. Höskuldsson, and T. Thordarson (2011), Dynamic magma mixing revealed by the 2010 Eyjafjallajökull eruption, *Solid Earth*, *2*, 271–281, doi:10.5194/se-2-271-2011.

Störmer, J. C., and J. Nicholls (1978), XLFRAC: A program for interactive testing of magmatic differentiation models, *Comput. Geosci.*, *87*, 51–64.

Straub, S. M., and G. D. Layne (2003), The systematics of chlorine, fluorine, and water in Izu arc front volcanic rocks: Implications for volatile recycling in subdution zones, *Geochim. Cosmochim. Acta*, *67*, 4179–4203, doi:10.1016/S0016-7037(03)00307-7.

Thordarson, T., and G. Larsen (2007), Volcanism in Iceland in historical time: Volcano types, eruption styles and eruptive history, *J. Geodyn.*, *43*, 118–152, doi:10.1016/j.jog.2006.09.005.

Thordarson, T., S. Self, N. Oskarsson, and T. Hulsebosh (1996), Sulfur, chlorine and fluorine degassing and atmospheric loading by the 1783–1784 AD Laki (Skaftar fires) eruption in Iceland, *Bull. Volcanol.*, *58*, 205–225, doi:10.1007/s004450050136.

Thordarson, T., S. Self, J. M. Miller, G. Larsen, and E. G. Vilmundardottir (2003), Sulphur release from flood lava eruptions in the Vedivötn, Grimsvötn and Katla volcanic sytems, Iceland, in *Volcanic Degassing*, edited by C. Oppenheimer et al., *Geol. Soc. Spec. Publ.*, *213*, 103–121.

Thordarson, T., C. Hayward, S. Moune, M. Hartley, O. Sigmarsson, Á. Höskuldsson, M. T. Guðmundsson, and F. Sigmundsson (2011), The 20 March–12 April 2010 Fimmvörðuháls eruption, Eyjafjallajöull volcano, Iceland: Volatile contents and magma degassing, *Geophys. Research Abstr.*, *13*, Abstract EGU2011-12147.

Thornber, C. R., D. R. Sherrod, D. F. Siems, C. C. Heliker, G. P. Meeker, R. L. Oscarson, and J. P. Kauahikaua (2002), Whole-rock and glass major-element chemistry of Kilauea Volcano, Hawaii, near-vent eruptive products: September 1994 through September 2001, *U.S. Geol. Surv. Open File Rep.*, *02-17*.

Toplis, M. J. (2005), The thermodynamics of iron and magnesium partitioning between olivine and liquid: Criteria for assessing and predicting equilibrium in natural and experimental systems, *Contrib. Mineral. Petrol.*, *149*, 22–39, doi:10.1007/s00410-004-0629-4.

J. K. Keiding, German Research Centre for Geosciences, Telegrafenberg, D-14473 Potsdam, Germany. (jakob@gfz-potsdam.de)

S. Moune and P. Schiano, Laboratoire Magmas et Volcans, Université Blaise Pascal, CNRS-IRD, F-63038 Clermont-Ferrand, France. (s.moune@opgc.univ-bpclermont.fr; p.schiano@opgc.univ-bpclermont.fr)

O. Sigmarsson, Institute of Earth Science, Nordvolc, University of Iceland, 101 Reykjavik, Iceland. (o.sigmarsson@opgc.univ-bpclermont.fr)

T. Thordarson, Grant Institute, School of GeoScience, University of Edinburgh, Edinburgh EH9 3JW, UK. (thor.thordarson@ed.ac.uk)